

Magnetic Dynamo Caused by Axions in Neutron Stars

Filippo Anzuini^{1,2,3,*} José A. Pons⁴ Antonio Gómez-Bañón⁴ Paul D. Lasky^{1,2}
 Federico Bianchini^{5,6,7} and Andrew Melatos^{3,8}

¹*School of Physics and Astronomy, Monash University, Clayton, Victoria 3800, Australia*

²*OzGrav: The ARC Centre of Excellence for Gravitational Wave Discovery, Clayton, Victoria 3800, Australia*

³*School of Physics, The University of Melbourne, Parkville, Victoria 3010, Australia*

⁴*Departament de Física Aplicada, Universitat d'Alacant, 03690 Alicante, Spain*

⁵*Kavli Institute for Particle Astrophysics and Cosmology, Stanford University, 452 Lomita Mall, Stanford, California, 94305, USA*

⁶*SLAC National Accelerator Laboratory, 2575 Sand Hill Road, Menlo Park, California, 94025, USA*

⁷*Department of Physics, Stanford University, 382 Via Pueblo Mall, Stanford, California, 94305, USA*

⁸*Australian Research Council Centre of Excellence for Gravitational Wave Discovery (OzGrav), The University of Melbourne, Parkville, Victoria 3010, Australia*

 (Received 10 August 2022; revised 19 November 2022; accepted 3 January 2023; published 15 February 2023)

The coupling between axions and photons modifies Maxwell's equations, introducing a dynamo term in the magnetic induction equation. In neutron stars, for critical values of the axion decay constant and axion mass, the magnetic dynamo mechanism increases the total magnetic energy of the star. We show that this generates substantial internal heating due to enhanced dissipation of crustal electric currents. These mechanisms would lead magnetized neutron stars to increase their magnetic energy and thermal luminosity by several orders of magnitude, in contrast to observations of thermally emitting neutron stars. To prevent the activation of the dynamo, bounds on the allowed axion parameter space can be derived.

DOI: [10.1103/PhysRevLett.130.071001](https://doi.org/10.1103/PhysRevLett.130.071001)

Introduction.—Axions were originally introduced to solve the strong CP problem [1–6]. Current constraints on axions are based on a wide range of techniques, from laboratory experiments to astrophysics [6–14]. Bounds on the axion parameter space are obtained using helioscopes or haloscopes [7,15–21], calculating axion emission in neutron stars (NSs) [22–25], and with other astrophysical and cosmological constraints [26–33].

It has been recently shown that finite density corrections change the axion field in NSs, which can become large compared with the vanishing expectation value in vacuo [34–37], and may mediate long-range forces in binary NS systems [34,35,38]. Under these conditions, additional observable effects can be used to constrain the axion parameter space.

In this Letter, we take advantage of these and other astrophysical aspects of NSs. The ultrastrong magnetic fields of NSs allow us to test axion electrodynamics beyond the strengths attainable in terrestrial laboratories. The axion-photon coupling introduces additional terms in Maxwell's equations [20,39,40]. In this Letter, we highlight that such coupling introduces a dynamo term in the magnetic induction equation, which can be used to place constraints on axion parameters, and to test models of axions in dense matter. By studying the specific case of crust-confined magnetic fields, we find that when the mass and decay constant of the axion reach critical thresholds, the dynamo supplies the star with additional magnetic

energy. As the magnetic field gets stronger, the stellar interior is heated up by enhanced dissipation of electric currents in the crust. This process increases the observable thermal luminosity, in tension with observations of thermally emitting, isolated NSs for a wide range of parameters.

To reconcile the presence of axions in the interior of NSs with observations, we appeal to one of the following scenarios: (i) the axion mass, decay constant, and axion-photon coupling constant (that determine the axion field profile in dense matter and regulate the interaction with electromagnetic fields) are below the critical values that activate the axion dynamo in the magnetized crust; (ii) a nonlinear saturation mechanism may halt the supply of magnetic energy via the dynamo beyond a certain threshold; or (iii) NSs do not source axions [34–36,38] (or they do not couple with photons).

Maxwell-axion equations.—Two sets of Maxwell's equations with axions are used in the literature: the set preserving the duality symmetry [40–42], and the “standard” set, often used in direct axion searches [15,20,39]. In this Letter, we employ the Maxwell-axion equations derived in [40]. The practical advantage is that the dynamo term appears explicitly in the magnetic induction equation. We simulate the magnetothermal evolution of NSs with an active axion dynamo, for highly and weakly magnetized stars (for the latter, see the Supplemental Material [43]) and for different initial magnetic configurations (see the

Supplemental Material [43]). The dynamo term is still present in the standard set of Maxwell's equations [15,39,44,45], which we study in the Supplemental Material [43] following Ref. [20].

We use an interior metric corresponding to a spherically symmetric, nonrotating body, with the notation $ds^2 = -e^{2\nu(r)}c^2dt^2 + e^{2\lambda(r)}dr^2 + r^2d\Omega^2$. In the absence of magnetic monopoles and magnetic currents, Maxwell's equations read as [40–42]

$$\nabla \cdot (\mathbf{E} - g_{a\gamma}a\mathbf{B}) = 4\pi\rho_c \quad (1a)$$

$$\nabla \times [e^\nu(\mathbf{B} + g_{a\gamma}a\mathbf{E})] = \frac{\partial(\mathbf{E} - g_{a\gamma}a\mathbf{B})}{c\partial t} + \frac{4\pi e^\nu}{c}\mathbf{J} \quad (1b)$$

$$\nabla \cdot (\mathbf{B} + g_{a\gamma}a\mathbf{E}) = 0 \quad (1c)$$

$$\nabla \times [e^\nu(\mathbf{E} - g_{a\gamma}a\mathbf{B})] = -\frac{1}{c}\frac{\partial(\mathbf{B} + g_{a\gamma}a\mathbf{E})}{\partial t}. \quad (1d)$$

In our notation, the ∇ operator includes the metric factors. Here, a is the axion field, ρ_c denotes the charge density, and \mathbf{J} is the electric current density. The axion-photon coupling is $g_{a\gamma} = g_\gamma\alpha_{\text{EM}}/\pi f_a$, where f_a is the axion decay constant, $g_\gamma = 0.37$ [5], and α_{EM} denotes the fine-structure constant.

Since we are interested in the long-term evolution on timescales of thousands to millions of years, and in the highly conductive NS interior $E \approx (v/c)\mathcal{B}$ (where $1 \text{ km/Myr} \lesssim v \lesssim 10^3 \text{ km/Myr}$ is the electron drift velocity in the crust), one can adopt some simplifying assumptions. In Eq. (1b), we neglect the term proportional to $\partial\mathbf{E}/\partial t$ (standard magnetohydrodynamics approximation) and $g_{a\gamma}\partial(a\mathbf{B})/\partial t$, which is typically much smaller than \mathbf{J} . We also use $\nabla \times (\mathbf{B} + g_{a\gamma}a\mathbf{E}) \approx \nabla \times \mathbf{B}$. In the induction equation, we neglect $g_{a\gamma}\partial(a\mathbf{E})/\partial t$. We check numerically that the terms above contribute with small or negligible corrections to the magnetic field evolution. We use the simplified version of Maxwell's equations below:

$$\nabla \cdot (\mathbf{E} - g_{a\gamma}a\mathbf{B}) = 4\pi\rho_c \quad (2a)$$

$$\nabla \times (e^\nu\mathbf{B}) = \frac{4\pi e^\nu}{c}\mathbf{J} \quad (2b)$$

$$\nabla \cdot \mathbf{B} = 0 \quad (2c)$$

$$\nabla \times [e^\nu(\mathbf{E} - g_{a\gamma}a\mathbf{B})] = -\frac{1}{c}\frac{\partial\mathbf{B}}{\partial t}. \quad (2d)$$

The system is closed with the electric field derived from a generalized Ohm's law [46]

$$\mathbf{E} = \frac{\mathbf{J}}{\sigma_e} + \frac{\mathbf{J} \times \mathbf{B}}{en_e c}, \quad (3)$$

where σ_e denotes the electric conductivity, while e and n_e denote the electric charge and the electron number density, respectively. Equation (3) is also employed in previous works on axions [42,44,45]. We expect σ_e to remain in the same range as in the case without axions, i.e., $\sigma_e \in [10^{22}, 10^{29}] \text{ s}^{-1}$ (see Figure 1 in Ref. [47] for the variation of σ_e in the crust). In such a range, $E \lesssim 10^{-15}\mathcal{B}$, which justifies the omission of terms such as $g_{a\gamma}\nabla \times (a\mathbf{E})$. Inserting the generalized Ohm's law in the induction equation, we get

$$\frac{\partial\mathbf{B}}{\partial t} = -\nabla \times [\eta\nabla \times (e^\nu\mathbf{B}) + f_H[\nabla \times (e^\nu\mathbf{B})] \times \mathbf{B} - g_{a\gamma}cae^\nu\mathbf{B}], \quad (4)$$

where $\eta = c^2/(4\pi\sigma_e)$ is the magnetic diffusivity and $f_H = c/(4\pi en_e)$. The first term in Eq. (4) accounts for Ohmic dissipation, and the second term for the Hall drift. The critical effect of axions is to include the third, *dynamolike* term. It may be interpreted as a dynamo or antidynamo, depending on the overall sign, and can increase or decrease, locally, the magnetic field strength (see the Supplemental Material [43] for the case of the standard axion-Maxwell equations [15,20]). The activation of the dynamo is regulated by the interplay of the Ohmic dissipative term, the Hall term, the magnitude of $g_{a\gamma}$, and of the axion gradient ∇a . Dynamos (without axions) also appear when simulating the magnetic field amplification in proto-NSs [48–51], such as in the case of the magneto-rotational instability with the α - Ω dynamo, or due to magnetized convection.

Axions in dense matter.—We now review the case of NSs sourcing axions. In Refs. [34–37] it is shown that, under certain conditions, the *in medio* axion potential has minima at $a/f_a \approx \pm\pi$, contrarily to the *in vacuo* potential, which is minimized at $a/f_a \approx 0$. The axion field profile in dense matter is the solution of the Klein-Gordon (KG) equation

$$\square a - \frac{\partial V}{\partial a} = \frac{g_{a\gamma}}{4\pi}\mathbf{E} \cdot \mathbf{B}, \quad (5)$$

where V is the *in medio* axion potential. *In vacuo*, the axion potential reads as [5,6]

$$V_0(a) = -m_\pi^2 f_\pi^2 \sqrt{1 - \frac{4m_u m_d}{(m_u + m_d)^2} \sin^2\left(\frac{a}{2f_a}\right)}, \quad (6)$$

where m_u and m_d are, respectively, the up and down quark masses, and $m_\pi = 135 \text{ MeV}$ and $f_\pi = 93 \text{ MeV}$ denote the mass of the neutral pion and the pion decay constant, respectively. Finite density corrections modify the axion potential, which in the linear approximation reads as [34,36,37]

$$V(a) \approx \left(1 - \frac{\sigma_N n_N}{m_\pi^2 f_\pi^2}\right) V_0(a), \quad (7)$$

where $\sigma_N = 59$ MeV and n_N is the nucleon number density. Different forms of the *in medio* axion potential have been derived [34–38]. We rely on the simple potential in Eq. (7) exclusively to determine where the shift of the axion field takes place (see below). This occurs above the nuclear saturation density, which may be caused by exotic phases in dense matter [36].

The key point in Refs. [34–36,38] is that the axion field is shifted to $a/f_a \approx \pm\pi$ at densities above a critical value, set by the condition that the prefactor $(1 - \sigma_N n_N/m_\pi^2 f_\pi^2)$ vanishes in the NS interior [34–37]. We denote the corresponding critical radius with $r = r_{\text{crit}}$. For $r > r_{\text{crit}}$, the axion field decreases exponentially on a length scale of the order of the inverse axion mass *in vacuo* m_a^{-1} [35,36], with $m_a = m_\pi f_\pi \sqrt{z}/[f_a(1+z)]$ (where $z = m_u/m_d \approx 0.48$ [5,37]).

Typically one has 10^8 GeV $\lesssim f_a \lesssim 10^{18}$ GeV and 10^{-11} eV $\lesssim m_a \lesssim 10^{-2}$ eV [6,12] for the QCD axion. For the parameters employed here ($f_a \approx 10^{15}$ GeV and $m_a \approx 10^{-9}$ eV) and typical NS magnetic field strengths, the electromagnetic backreaction on the axion field in the KG equation is negligible compared with the potential term, and the latter gives a stiff source. The solution to the KG equation is a field that oscillates with a frequency close to its Compton frequency, i.e., on a timescale far shorter than the typical, secular timescales for the NS magnetothermal evolution. On such long timescales, only the axion profile time averaged over several oscillations plays a role, and it shows negligible deviations from the stationary profile (\lesssim few parts in 10^4). We approximate the latter as in Ref. [36], i.e.,

$$a(r) \approx \begin{cases} \pm\pi f_a & r \leq r_{\text{crit}} \\ \pm\pi f_a \frac{r_{\text{crit}}}{r} e^{-m_a(r-r_{\text{crit}})} & r > r_{\text{crit}}. \end{cases} \quad (8)$$

Below we employ $a/f_a = \pi$ at high densities. We stress that the numerical results presented in this Letter rely on Eq. (8), and on the values of f_a , m_a , and r_{crit} .

The potential shift ΔV due to the sourcing of the axion field is $\Delta V \approx (m_\pi f_\pi)^2$ (for $a \approx \pi f_a$) [34,36], and allows us to determine an upper limit to the magnetic energy that the dynamo can convert, which amounts approximately to $\lesssim 10\%$ of the NS binding energy [52], and exceeds by orders of magnitude the magnetic energy expected in magnetars. However, for energies comparable to those of magnetars ($\approx 10^{48}$ – 10^{49} erg), the backreaction on the axion field and nonlinear saturation mechanisms may become important and may halt the growth of the magnetic energy.

The dynamo is active as long as ∇a is maintained in the magnetized region of the star, and operates on a timescale $\tau_{\text{dyn}} \approx |g_{a\gamma} c \nabla a|^{-1}$ [cf. Eq. (4)]. Given the axion exponential

profile in Eq. (8), τ_{dyn} varies by several orders of magnitude, depending on f_a . As shown below, the dynamo can make an observable difference for isolated NSs when τ_{dyn} is shorter than the typical cooling timescale (~ 1 Myr), which in the crust occurs for $f_a \gtrsim 3.6 \times 10^{15}$ GeV.

The dynamo mechanism.—We employ the two-dimensional, axisymmetric magnetothermal evolution numerical code for NSs developed by the Alicante group [46,53–58], recently modified to include hyperon species (GM1A equation of state [59]) in Refs. [60,61]. We consider a NS with mass $M = 1.8 M_\odot$ with superfluid nucleons and hyperons, with electrons, muons, and an iron-only outer envelope (cf. Refs. [60,61] for details, and Refs. [62–64] for superfluidity in NSs). In principle, the equation of state and several microphysical details are affected by a large axion field. However, the magnetic evolution is insensitive to such changes. Indeed, NS models obtained with different equations of state without axions (and hence with different structural and compositional properties, cf. for example, Refs. [57,58] with Refs. [60,61]) have a similar magnetic evolution, and we expect the same for equations of state including axions. Hence, we include the effect of axions only via Maxwell’s equations. Below, we focus on the A2 initial, crust-confined magnetic configuration, with a dipolar-poloidal, quadrupolar-toroidal field (see Table I). Other configurations (both crust-confined and core-threading) are considered in the Supplemental Material [43].

The total magnetic energy $E_{\text{tot}}^{\text{mag}}$ and the redshifted thermal luminosity L_γ of the NS model are displayed in Fig. 1. Panel (a) reports the evolution of $E_{\text{tot}}^{\text{mag}}$ for stars sourcing axions (blue, red, and orange curves) and without axions (green curve). To improve the stability of the simulations, we choose f_a such that $E_{\text{tot}}^{\text{mag}}$ grows on secular timescales. The dynamo supplies magnetic energy in the crust at a faster pace than the dissipative processes can reduce it. The higher f_a is, the shorter τ_{dyn} is. For the orange curve, $E_{\text{tot}}^{\text{mag}}$ is 2 orders of magnitude higher than the model without axions after $10^{4.5}$ yr.

TABLE I. Initial magnetic field configurations considered in this Letter. The polar surface strength of the dipolar-poloidal field is B_{dip} . $E_{\text{tor}}^{\text{mag}}$ and $E_{\text{tot}}^{\text{mag}}$ are the toroidal and total magnetic energy respectively. l_{pol} denotes the number of poloidal multipoles. All the magnetic configurations are crust confined, except for the C1 configuration. The latter includes also a toroidal field in the core region confined to an equatorial torus.

Configuration	B_{dip}	$E_{\text{tor}}^{\text{mag}}/E_{\text{tot}}^{\text{mag}}$	l_{pol}
A0	1.0×10^{10} G	93%	1
A1 $m_{2,2}$	1.0×10^{13} G	77%	2
A1	5.0×10^{13} G	35%	1
A2	3.0×10^{13} G	0	1
C1	2.0×10^{13} G	43%	1

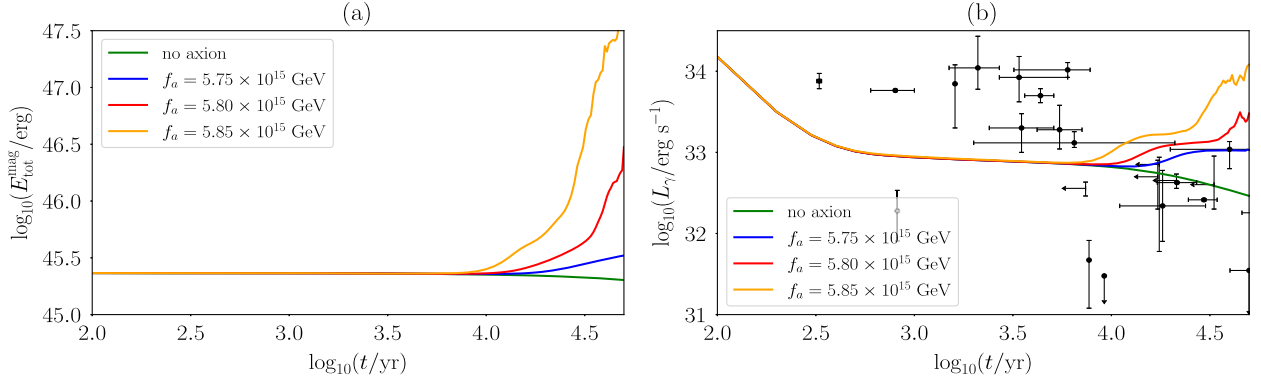


FIG. 1. Magnetic energy (a) and redshifted thermal luminosity L_γ (b) versus stellar age for different values of f_a and for the A2 initial magnetic configuration (cf. Table I). The black points correspond to thermally emitting, isolated NSs with inferred fields below 10^{14} G (taken from Ref. [65]).

Figure 1(b) shows the corresponding cooling curves. NSs without axions match the data of thermally emitting, isolated NSs with inferred fields $\lesssim 10^{14}$ G at $\gtrsim 10^4$ yr [65] (stronger initial fields match younger sources, cf. the Supplemental Material [43]). In NSs sourcing axions, the dissipation of intense electric currents that sustain the growing magnetic field enhances the Joule heating rate, increasing L_γ . In general, models without axions overlap with the data for $\lesssim 1$ Myr (see Refs. [60,61]); models with axions overshoot the observed L_γ of several sources with $L_\gamma \lesssim 10^{33}$ erg/s. We expect however L_γ to

saturate to a certain level, set by the balance between Joule heating and cooling processes ($> 10^{33}$ erg/s for the parameters employed here).

In Figure 2 we display the magnetothermal maps of a NS without axions (top panels) and with axions for $f_a = 5.8 \times 10^{15}$ GeV (bottom panels). The left hemispheres show the contours of the toroidal field $\mathbf{B}_{\text{tor}} = B_\phi \hat{\phi}$. Overplotted are the poloidal field lines (projected onto the meridional plane). The right hemispheres display the redshifted internal temperature T_i . The dynamo mechanism produces rich dynamics in the bottom panels. At

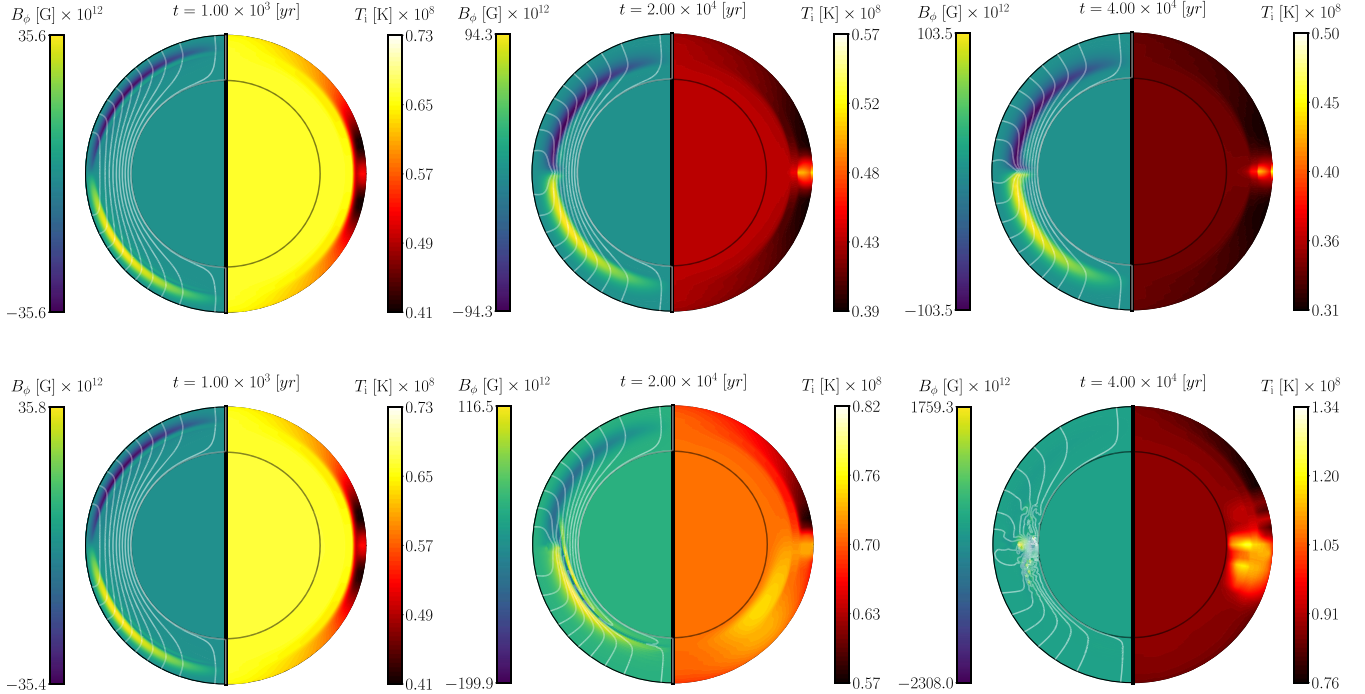


FIG. 2. Magnetic and temperature maps for the A2 configuration. The top panels correspond to a star that does not source axions; the bottom panels to a star sourcing an axion field with $f_a = 5.8 \times 10^{15}$ GeV. The maps extend from the NS center to the bottom of the outer envelope, i.e., the latter is not included in the plots. The crust is enlarged by a factor of 8 for visualization purposes. The scales in the colorbars change in time to preserve a high level of detail.

$t = 4 \times 10^4$ yr, B_ϕ is approximately 1 order of magnitude stronger for a star with axions (bottom panel) than for a star without axions (top panel). The temperature map shows that enhanced Joule heating due to the dynamo raises T_i at the equator with respect to the top panel.

We stress that, due to unavoidable theoretical and numerical limitations [66–71], there is a limited capability to reproduce realistic NS magnetic field configurations, where small-scale fields (which enhance Ohmic dissipation) may be endemic. However, a slight increase of f_a promotes the efficiency of the dynamo, so that the f_a values studied here should remain valid even with more complex configurations. We also note that such values of f_a allow us to test $g_{a\gamma} \approx 10^{-19}$ GeV $^{-1}$, which is orders of magnitude smaller than the sensitivity of ADMX ($g_{a\gamma} \approx 10^{-16}$ GeV $^{-1}$ [21]).

Conclusion.—NSs are ideal environments to test axion electrodynamics, and can be used to derive constraints on the axion parameter space, complementing ground-based axion searches [7,8,11,20,21], and to assess proposed axion models [34–38].

We find that the coupling of axions with photons leads to the appearance of a magnetic dynamo term in the magnetic induction equation. In NSs sourcing axions with $a \approx \pm\pi f_a$ [34–36], the magnetic energy of the star increases by orders of magnitude, for certain threshold values of the axion decay constant and axion mass. The thermal luminosity L_γ increases by roughly 1 order of magnitude with respect to NSs without axions due to enhanced dissipation of the strong electric currents that sustain the growing magnetic field. Values of L_γ in the range $\gtrsim 10^{33}$ erg/s maintained by the dynamo are in tension with available data, in particular with mature NSs with ages $\gtrsim 10^4$ yr and $L_\gamma \lesssim 10^{33}$ erg/s [65].

The activation of the dynamo may be prevented under certain conditions. It does not activate if f_a and m_a are such that the dynamo term is sufficiently small in the magnetized crust. Moreover, one cannot exclude *a priori* an efficient mechanism, which may saturate the magnetic energy of the star beyond a certain threshold. Another possibility is that the axion field is not shifted to $a \approx \pm\pi f_a$ in NS interiors [34–38].

We conclude with some caveats. The results presented in this Letter are calculated using the axion profile in Eq. (8), which is an approximate solution to the KG equation. Moreover, in realistic NS magnetic field configurations, Ohmic dissipation may be enhanced due to the presence of small-scale fields. However, a slight change in f_a increases the efficiency of the dynamo, so that the range of f_a studied in this Letter is expected to remain similar even in the presence of more complex configurations.

F. A. thanks Koichi Hamaguchi, Reuven Balkin, Hugo Terças, David J. E. Marsh, and Angelo Maggi for valuable discussions. F. A., P. D. L., and A. M. are supported by the Australian Research Council (ARC) Centre of Excellence for Gravitational Wave Discovery (OzGrav), through

Project No. CE170100004. P. D. L. is supported through ARC Discovery Project No. DP220101610. J. A. P. acknowledges support by the Generalitat Valenciana (PROMETEO/2019/071) and AEI Grant No. PID2021-127495NB-I00.

*filippo.anzuini@gmail.com

- [1] R. D. Peccei and H. R. Quinn, *CP Conservation in the Presence of Pseudoparticles*, *Phys. Rev. Lett.* **38**, 1440 (1977).
- [2] R. D. Peccei and H. R. Quinn, Constraints imposed by *CP* conservation in the presence of pseudoparticles, *Phys. Rev. D* **16**, 1791 (1977).
- [3] F. Wilczek, Problem of Strong *p* and *t* Invariance in the Presence of Instantons, *Phys. Rev. Lett.* **40**, 279 (1978).
- [4] S. Weinberg, A New Light Boson?, *Phys. Rev. Lett.* **40**, 223 (1978).
- [5] G. G. di Cortona, E. Hardy, J. P. Vega, and G. Villadoro, The QCD axion, precisely, *J. High Energy Phys.* **01** (2016) 034.
- [6] L. Di Luzio, M. Giannotti, E. Nardi, and L. Visinelli, The landscape of QCD axion models, *Phys. Rep.* **870**, 1 (2020).
- [7] S. J. Asztalos, G. Carosi, C. Hagmann, D. Kinion, K. van Bibber, M. Hotz, L. J. Rosenberg, G. Rybka, J. Hoskins, J. Hwang, P. Sikivie, D. B. Tanner, R. Bradley, J. Clarke (ADMX Collaboration), SQUID-Based Microwave Cavity Search for Dark-Matter Axions, *Phys. Rev. Lett.* **104**, 041301 (2010).
- [8] D. Budker, P. W. Graham, M. Ledbetter, S. Rajendran, and A. O. Sushkov, Proposal for a Cosmic Axion Spin Precession Experiment (CASPER), *Phys. Rev. X* **4**, 021030 (2014).
- [9] A. Arvanitaki and A. A. Geraci, Resonantly Detecting Axion-Mediated Forces with Nuclear Magnetic Resonance, *Phys. Rev. Lett.* **113**, 161801 (2014).
- [10] Y. Kahn, B. R. Safdi, and J. Thaler, Broadband and Resonant Approaches to Axion Dark Matter Detection, *Phys. Rev. Lett.* **117**, 141801 (2016).
- [11] V. Anastassopoulos *et al.* (CAST Collaboration), New CAST limit on the axion-photon interaction, *Nat. Phys.* **13**, 584 (2017).
- [12] I. G. Irastorza and J. Redondo, New experimental approaches in the search for axion-like particles, *Prog. Part. Nucl. Phys.* **102**, 89 (2018).
- [13] L. Di Luzio, J. Galan, M. Giannotti, I. G. Irastorza, J. Jaeckel, A. Lindner, J. Ruz, U. Schneekloth, L. Sohl, L. J. Thormaehlen, and J. K. Vogel, Probing the axion-nucleon coupling with the next generation of axion helioscopes, *Eur. Phys. J. C* **82**, 120 (2022).
- [14] M. J. Dolan, F. J. Hiskens, and R. R. Volkas, Advancing globular cluster constraints on the axion-photon coupling, *J. Cosmol. Astropart. Phys.* **10** (2022) 096.
- [15] P. Sikivie, Experimental Tests of the “Invisible” Axion, *Phys. Rev. Lett.* **51**, 1415 (1983).
- [16] P. Sikivie, Experimental Tests of the “Invisible” Axion, *Phys. Rev. Lett.* **52**, 695 (1984).
- [17] C. Hagmann, P. Sikivie, N. Sullivan, D. B. Tanner, and S. Cho, Cavity design for a cosmic axion detector, *Rev. Sci. Instrum.* **61**, 1076 (1990).

- [18] N. Du *et al.* (ADMX Collaboration), Search for Invisible Axion Dark Matter with the Axion Dark Matter Experiment, *Phys. Rev. Lett.* **120**, 151301 (2018).
- [19] S. Knirck, J. Schütte-Engel, A. Millar, J. Redondo, O. Reimann, A. Ringwald, and F. Steffen, A first look on 3D effects in open axion haloscopes, *J. Cosmol. Astropart. Phys.* **08** (2019) 026.
- [20] Y. Kim, D. Kim, J. Jeong, J. Kim, Y. C. Shin, and Y. K. Semertzidis, Effective approximation of electromagnetism for axion haloscope searches, *Phys. Dark Universe* **26**, 100362 (2019).
- [21] T. Braine *et al.* (ADMX Collaboration), Extended Search for the Invisible Axion with the Axion Dark Matter Experiment, *Phys. Rev. Lett.* **124**, 101303 (2020).
- [22] A. Sedrakian, Axion cooling of neutron stars, *Phys. Rev. D* **93**, 065044 (2016).
- [23] K. Hamaguchi, N. Nagata, K. Yanagi, and J. Zheng, Limit on the axion decay constant from the cooling neutron star in Cassiopeia A, *Phys. Rev. D* **98**, 103015 (2018).
- [24] A. Sedrakian, Axion cooling of neutron stars. II. Beyond hadronic axions, *Phys. Rev. D* **99**, 043011 (2019).
- [25] M. Buschmann, C. Dessert, J. W. Foster, A. J. Long, and B. R. Safdi, Upper Limit on the QCD Axion Mass from Isolated Neutron Star Cooling, *Phys. Rev. Lett.* **128**, 091102 (2022).
- [26] G. G. Raffelt, Astrophysical axion bounds, *Lect. Notes Phys.* **741**, 51 (2008).
- [27] L. B. Leinson, Axion mass limit from observations of the neutron star in cassiopeia a, *J. Cosmol. Astropart. Phys.* **08** (2014) 031.
- [28] D. J. E. Marsh, Axion cosmology, *Phys. Rep.* **643**, 1 (2016).
- [29] B. Garbrecht and J. I. McDonald, Axion configurations around pulsars, *J. Cosmol. Astropart. Phys.* **07** (2018) 044.
- [30] F. V. Day and J. I. McDonald, Axion superradiance in rotating neutron stars, *J. Cosmol. Astropart. Phys.* **01** (2019) 051.
- [31] M. J. Dolan, F. J. Hiskens, and R. R. Volkas, Constraining axion-like particles using the white dwarf initial-final mass relation, *J. Cosmol. Astropart. Phys.* **09** (2021) 010.
- [32] L. D. Luzio, M. Fedele, M. Giannotti, F. Mescia, and E. Nardi, Stellar evolution confronts axion models, *J. Cosmol. Astropart. Phys.* **02** (2022) 035.
- [33] C. Balázs, S. Bloor, T. E. Gonzalo, W. Handley, S. Hoof, F. Kahlhoefer, M. Lacroix, D. J. E. Marsh, J. J. Renk, P. Scott, and P. Stöcker, Cosmological constraints on decaying axion-like particles: A global analysis, *J. Cosmol. Astropart. Phys.* **12** (2022) 027.
- [34] A. Hook and J. Huang, Probing axions with neutron star inspirals and other stellar processes, *J. High Energy Phys.* **06** (2018) 036.
- [35] J. Huang, M. C. Johnson, L. Sagunski, M. Sakellariadou, and J. Zhang, Prospects for axion searches with Advanced LIGO through binary mergers, *Phys. Rev. D* **99**, 063013 (2019).
- [36] R. Balkin, J. Serra, K. Springmann, and A. Weiler, The QCD axion at finite density, *J. High Energy Phys.* **07** (2020) 221.
- [37] L. Di Luzio, B. Gavela, P. Quilez, and A. Ringwald, An even lighter QCD axion, *J. High Energy Phys.* **05** (2021) 184.
- [38] J. Zhang, Z. Lyu, J. Huang, M. C. Johnson, L. Sagunski, M. Sakellariadou, and H. Yang, First Constraints on Nuclear Coupling of Axionlike Particles from the Binary Neutron Star Gravitational Wave Event GW170817, *Phys. Rev. Lett.* **127**, 161101 (2021).
- [39] F. Wilczek, Two Applications of Axion Electrodynamics, *Phys. Rev. Lett.* **58**, 1799 (1987).
- [40] L. Visinelli, Axion-electromagnetic waves, *Mod. Phys. Lett. A* **28**, 1350162 (2013).
- [41] B. R. Ko, H. Themann, W. Jang, J. Choi, D. Kim, M. J. Lee, J. Lee, E. Won, and Y. K. Semertzidis, Electric and magnetic energy at axion haloscopes, *Phys. Rev. D* **94**, 111702(R) (2016).
- [42] H. Terças, J. D. Rodrigues, and J. T. Mendonça, Axion-Plasmon Polaritons in Strongly Magnetized Plasmas, *Phys. Rev. Lett.* **120**, 181803 (2018).
- [43] See Supplemental Material at <http://link.aps.org/supplemental/10.1103/PhysRevLett.130.071001> for details and additional results for the axion dynamo.
- [44] A. J. Long and T. Vachaspati, Implications of a primordial magnetic field for magnetic monopoles, axions, and Dirac neutrinos, *Phys. Rev. D* **91**, 103522 (2015).
- [45] I. Rogachevskii, O. Ruchayskiy, A. Boyarsky, J. Fröhlich, N. Kleeorin, A. Brandenburg, and J. Schober, Laminar and turbulent dynamos in chiral magnetohydrodynamics. I. Theory, *Astrophys. J.* **846**, 153 (2017).
- [46] J. A. Pons and D. Viganò, Magnetic, thermal and rotational evolution of isolated neutron stars, *Living Rev. Comput. Astrophys.* **5**, 3 (2019).
- [47] J. A. Pons and U. Geppert, Magnetic field dissipation in neutron star crusts: From magnetars to isolated neutron stars, *Astron. Astrophys.* **470**, 303 (2007).
- [48] C. Thompson and R. C. Duncan, Neutron star dynamos and the origins of pulsar magnetism, *Astrophys. J.* **408**, 194 (1993).
- [49] A. Bonanno, V. Urpin, and G. Belvedere, Protoneutron star dynamos and pulsar magnetism, *Astron. Astrophys.* **440**, 199 (2005).
- [50] L. Naso, L. Rezzolla, A. Bonanno, and L. Paternò, Magnetic field amplification in proto-neutron stars. The role of the neutron-finger instability for dynamo excitation, *Astron. Astrophys.* **479**, 167 (2008).
- [51] A. Reboul-Salze, J. Guilet, R. Raynaud, and M. Bugli, MRI-driven $\alpha - \Omega$ dynamos in protoneutron stars, *Astron. Astrophys.* **667**, A94 (2022).
- [52] J. M. Lattimer and M. Prakash, Neutron star structure and the equation of state, *Astrophys. J.* **550**, 426 (2001).
- [53] D. N. Aguilera, J. A. Pons, and J. A. Miralles, 2D cooling of magnetized neutron stars, *Astron. Astrophys.* **486**, 255 (2008).
- [54] J. A. Pons, J. A. Miralles, and U. Geppert, Magneto-thermal evolution of neutron stars, *Astron. Astrophys.* **496**, 207 (2009).
- [55] D. Viganò, J. A. Pons, and J. A. Miralles, A new code for the Hall-driven magnetic evolution of neutron stars, *Comput. Phys. Commun.* **183**, 2042 (2012).
- [56] D. Viganò, N. Rea, J. Pons, R. Perna, D. Aguilera, and J. Miralles, Unifying the observational diversity of isolated neutron stars via magneto-thermal evolution models, *Mon. Not. R. Astron. Soc.* **434**, 123 (2013).

- [57] C. Dehman, D. Viganò, N. Rea, J. A. Pons, R. Perna, and A. Garcia-Garcia, On the rate of crustal failures in young magnetars, *Astrophys. J. Lett.* **902**, L32 (2020).
- [58] D. Viganò, A. Garcia-Garcia, J. A. Pons, C. Dehman, and V. Graber, Magneto-thermal evolution of neutron stars with coupled Ohmic, Hall and ambipolar effects via accurate finite-volume simulations, *Comput. Phys. Commun.* **265**, 108001 (2021).
- [59] M. E. Gusakov, P. Haensel, and E. M. Kantor, Physics input for modelling superfluid neutron stars with hyperon cores, *Mon. Not. R. Astron. Soc.* **439**, 318 (2014).
- [60] F. Anzuini, A. Melatos, C. Dehman, D. Viganò, and J. A. Pons, Fast cooling and internal heating in hyperon stars, *Mon. Not. R. Astron. Soc.* **509**, 2609 (2021).
- [61] F. Anzuini, A. Melatos, C. Dehman, D. Viganò, and J. A. Pons, Thermal luminosity degeneracy of magnetized neutron stars with and without hyperon cores, *Mon. Not. R. Astron. Soc.* **515**, 3014 (2022).
- [62] G. Baym, C. Pethick, and D. Pines, Superfluidity in neutron stars, *Nature (London)* **224**, 673 (1969).
- [63] A. Sedrakian and J. W. Clark, Superfluidity in nuclear systems and neutron stars, *Eur. Phys. J. A* **55**, 167 (2019).
- [64] T. S. Wood, V. Graber, and W. G. Newton, Superconducting phases in a two-component microscale model of neutron star cores, [arXiv:2011.02873](https://arxiv.org/abs/2011.02873).
- [65] A. Y. Potekhin, D. A. Zyuzin, D. G. Yakovlev, M. V. Beznogov, and Y. A. Shibano, Thermal luminosities of cooling neutron stars, *Mon. Not. R. Astron. Soc.* **496**, 5052 (2020).
- [66] J. Braithwaite and H. C. Spruit, Evolution of the magnetic field in magnetars, *Astron. Astrophys.* **450**, 1097 (2006).
- [67] S. K. Lander and D. I. Jones, Magnetic fields in axisymmetric neutron stars, *Mon. Not. R. Astron. Soc.* **395**, 2162 (2009).
- [68] K. N. Gourgouliatos, A. Cumming, A. Reisenegger, C. Armaza, M. Lyutikov, and J. A. Valdivia, Hall equilibria with toroidal and poloidal fields: application to neutron stars, *Mon. Not. R. Astron. Soc.* **434**, 2480 (2013).
- [69] K. N. Gourgouliatos, T. S. Wood, and R. Hollerbach, Magnetic field evolution in magnetar crusts through three-dimensional simulations, *Proc. Natl. Acad. Sci. U.S.A.* **113**, 3944 (2016).
- [70] T. S. Wood and R. Hollerbach, Three Dimensional Simulation of the Magnetic Stress in a Neutron Star Crust, *Phys. Rev. Lett.* **114**, 191101 (2015).
- [71] A. P. Igoshev, R. Hollerbach, T. Wood, and K. N. Gourgouliatos, Strong toroidal magnetic fields required by quiescent X-ray emission of magnetars, *Nat. Astron.* **5**, 145 (2021).